arXiv:1403.6325v1 [astro-ph.SR] 25 Mar 2014

The Clusters AgeS Experiment (CASE). VI. Analysis of two detached eclipsing binaries in the Globular Cluster M55*

J. Kaluzny[1], I. B. Thompson[2], A. Dotter[3] M. Rozyczka[1], W. Pych[1] S. M. Rucinski[4], and G. S. Burley[2]

[1]Nicolaus Copernicus Astronomical Center, ul. Bartycka 18, 00-716 Warsaw, Poland
e-mail: (jka, mnr, wp)@camk.edu.pl
[2]The Observatories of the Carnegie Institution of Washington, 813 Santa Barbara Street, Pasadena, CA 91101, USA
e-mail: ian@obs.carnegiescience.edu
[3]Research School of Astronomy and Astrophysics, Australian National University, Canberra, Australia
e-mail: dotter@mso.anu.edu.au
[4]Department of Astronomy and Astrophysics, University of Toronto, 50 St. George Street, Toronto, ON M5S 3H4, Canada
e-mail: rucinski@astro.utoronto.ca

ABSTRACT

We present an analysis of the detached eclipsing binaries V44 and V54 belonging to the globular cluster M55. For V54 we obtain the following absolute parameters: $M_p = 0.726 \pm 0.015 M_\odot$, R_p=1.006±0.009$R_\odot$, L_p=1.38±0.07$L_\odot$ for the primary, and M_s=0.555±0.008$M_\odot$, $R_s = 0.528 \pm 0.005\, R_\odot$, $L_s = 0.16 \pm 0.01\, L_\odot$ for the secondary. The age and apparent distance modulus of V54 are estimated at 13.3 – 14.7 Gyr and 13.94 ± 0.05 mag, respectively. This derived age is substantially larger than ages we have derived from the analysis of binary systems in 47 Tuc and M4. The secondary of V44 is so weak in the optical domain that only mass function and relative parameters are obtained for the components of this system. However, there is a good chance that the velocity curve of the secondary could be derived from near-IR spectra. As the primary of V44 is more evolved than that of V54, such data would impose much tighter limits on the age and distance of M55.

binaries: close binaries: spectroscopic globular clusters: individual (M55) stars: individual (V44-M55, V54-M55)

1 Introduction

The general goal of the Cluster AgeS Experiment (CASE) is to determine the basic stellar parameters (masses, luminosities, and radii) of the components of globular cluster binaries to a precision better than 1% in order to measure ages and distances of their parent clusters, and to test stellar evolution models (Kaluzny et al. 2005). Within the CASE series, this is the third paper devoted to the study of detached eclipsing binaries (DEBs) with main-sequence or subgiant components. In the previous two papers we analyzed three such systems in M4 (Kaluzny et al. 2013) and another one in 47 Tuc (Thompson et al. 2010). The eclipsing binaries M55-V44 and M55-V54 (henceforth V44 and V54) were

*Based on data obtained with the Magellan, du Pont, and Swope telescopes Las Campanas Observatory.

discovered in the field of the globular cluster M55 (Kaluzny et al. 2010). Follow-up spectroscopy indicated that both systems are radial velocity members of the cluster, and their membership was confirmed by the proper motion study of Zloczewski et al. (2012).

V44 and V54 are located in the turn-off region on the color-magnitude diagram (CMD) of the cluster. With orbital periods of 2.17 d and 9.27 d they are well detached, and their analysis can provide interesting constraints on the age and distance of M55. In this paper we analyze light and velocity curves of the SB2 system V54 and determine the absolute parameters of its components. We also obtain the mass function and a light-curve solution of the SB1 system V44. THe photometric and spectroscopic data are described in Section 2. The analysis of the data is detailed in Section 3. The age and distance of M55 are derived in Section 4, and our results are summarized in Section 5.

2 Observations

2.1 Photometry

The first eclipses of V44 and V54 were detected in 1997 during the survey part of the CASE project. For the survey we used the 1-m Swope telescope equipped with the SITE3 2048×3150 pixel CCD camera. Observations of the cluster extended from 1997 to 2009. About 80% and 20% of the data were taken in V and B bands, respectively. At a scale of 0.435 arcsec/pixel, most of the collected images were adequately sampled. For frames taken with the V filter the median seeing was 1.45 arcsec.

Profile photometry was extracted with the DoPHOT package (Schechter et al. 1993), following the approach of Kaluzny et al. (1999). Another set of frames was collected between 1997 and 2009 using the 2.5-m du Pont telescope and the 2048^2 pixel TEK5 CCD camera. These observations and their reductions were described in detail by Kaluzny et al. (2010). Here we note that the time-series BV photometry was performed with the image-subtraction method. In June 2010 the primary eclipse of V54 was additionally observed with the du Pont telescope equipped with the 2048^2 pixel SITE2K CCD camera. All the data were calibrated onto the standard BV system.

Altogether, several primary eclipses were observed for both V44 and V54. However, only for some of them were both branches (ingress and egress) covered, allowing for a precise timing. Secondary eclipses of V44 and V54 are shallow and we decided not to use them for period determination. Moments of primary minima were obtained using the KWALEX code kindly provided by Alex Schwarzenberg-Czerny. The O$-$C residuals listed in Table 1 are based on the following linear ephemerides:

$$\begin{aligned} HJD^{\rm V44}_{\rm min} &= 2452076.86240(47) + 2.16612156(49) \times E \\ HJD^{\rm V54}_{\rm min} &= 2450663.6766(17) + 9.2691537(36) \times E, \end{aligned} \qquad (1)$$

where numbers in parentheses are the uncertainties of the last two significant digits. In both systems we found no evidence for any variability of the orbital period. Moreover, within the errors the same values for the periods were derived by applying the Kinmann-Lafler algorithm (Lafler & Kinman 1965) to complete light curves including partially covered eclipses. Light curves obtained from du Pont/TEK5 data and phased with the ephemerides (1) are shown in Fig. 1.

Data obtained with the SITE2K CCD camera were used solely to find times of minima.

2.2 Spectroscopy

Our radial velocity data are based on observations performed with the MIKE Echelle spectrograph (Bernstein et al. 2003) on the Magellan Clay telescope between July 18th, 2003 and July 12th, 2010 (UT). Most of the observations consisted of two 1800 s exposures interlaced with an exposure of a Th/Ar lamp (depending on observing conditions, some exposures were shorter or longer). For all observations a 0.7×5.0 arcsec slit was used, and 2×2 pixel binning was applied. For λ=438 nm the resolution was $\sim$2.7 pixels at a scale of 0.0043 nm/pixel. The spectra were processed using a pipeline developed by Dan Kelson following the formalism of Kelson (2003).

In the blue channel of MIKE (380 – 500 nm) the typical S/N ratio at 440 nm was 12 for both V44 and V54. The S/N ratios for the red channel (490 – 1000 nm) spectra were markedly worse, and so only data from the blue channel were used for radial velocity measurements. For V54 the velocities were measured using software based on the TODCOR algorithm of Zucker & Mazeh (1994), kindly made available by Guillermo Torres. Synthetic echelle-resolution spectra from the library of Coelho et al. (2005), interpolated to log$g$ and T_{eff} taken from the photometric solution, were used as velocity templates. The templates were Gaussian-smoothed to match the resolution of the observed spectra. We adopted [Fe/H]$=-2.0$ and [α/Fe]$=+0.4$ for the chemical composition (Harris 1996; 2010 electronic version). The average α-element to Fe ratios in this cluster have been determined from UVES spectra of 14 red giant stars to be [Mg/Fe]$=+0.47$, [Si/Fe]$=+0.38$, and [Ca/Fe]$=+0.36$ (Carretta et al. 2009, 2010). All velocities were measured on the wavelength range 400 – 460 nm. The results of the velocity measurements of V54 are presented in Table 2. In the case of V44 even the best spectra showed only a marginal signal from the secondary component in the cross correlation function, so that velocities have been measured for the primary component only. These were derived with the IRAF/FXCOR[†] task and are listed in Table 3.

3 Analysis of light and radial velocity curves

The light curves were analysed with the PHOEBE implementation (Prša et al. 2005) of the Wilson-Devinney model (Wilson & Devinney 1971; Wilson 1979). Linear limb darkening coefficients were interpolated from the tables of Claret (2000) with the help of the JKTLD code.[‡]. The effective temperatures of the primary components were estimated based on their dereddened $B-V$ colors. Since the existing empirical calibrations are rather poorly defined for cool low-metallicity stars (see, e.g., Figs. 13 and 14 in Casagrande et al. 2010), we employed a theoretical calibration based on models of Castelli & Kurucz (2004; hereafter CK). For the reddening of M55 we adopted $E(B-V) = 0.115 \pm 0.010$ mag, a value 0.035 mag larger than that listed in the catalog of Harris (1996). This choice is based on the determinations of Richter et al. (1999) and Dotter et al. (2010), who quote $E(B-V) = 0.11 \pm 0.02$ mag and $E(B-V) = 0.115$

[†] [1]IRAF is distributed by the National Optical Astronomy Observatories, which are operated by the AURA, Inc., under cooperative agreement with the NSF.

[‡]Written by John Southworth and available at www.astro.keele.ac.uk/jkt/codes/jktld.html

mag, respectively. The map of galactic extinction by Schlegel et al. (1998) predicts $E(B-V)=0.136$ mag for M55; however, it is known to systematically overestimate the reddening (Schlafly et al. 2010). Recently, a detailed reddening map for the region of Corona Australis complex including M55 was presented by Alves et al. (2014). Their map is based on 2MASS data and has a resolution of 3 arcmin. As it turns out, the projected position of M55 coincides with the northeast edge of the Pipe Nebula, see their Figs. 2 and 3. This map implies in particular that there is some differential reddening across the cluster field, with extinction decreasing from west to east. This is in fact consistent with our BV photometry based on the du Pont/TEK5 data, which covers the central 8 arcmin of the cluster area. As one may note from Fig. 3, the cluster turnoff is redder by $\approx$0.01 mag in the region around V54 than around V44. Dr. Alves kindly communicated to us that the average reddening around the whole cluster amounts to $A_V = 0.30 \pm -0.01$, assuming $A_V = 8.9 \times A_K$. This in turn corresponds to $E(B-V)=0.097\pm0.003$ for the standard extinction ratio of 3.1. Given the fact V54 is located in the western part of M55 our adopted reddening of $E(B-V) = 0.11$ is consistent with results of Alves et al. (2014). A more detailed analysis of this subject has to be postponed till the reddening map is published. The total errors of the dereddened colors listed in Table 4 include a 0.01 mag uncertainty in the zero points of our BV photometry.

The light curves were phased with the ephemerides given by eq. (1). For V54 we adjusted the inclination i, relative radii r_p and r_s, effective temperature of the secondary T_s, eccentricity e and periastron longitude ω. In the case of V44 we assumed a circular orbit, so that only the first four parameters were adjusted. V and B curves were solved simultaneously. The standard 1-σ errors of the PHOEBE solution given in Table 4 were found using a Monte Carlo procedure written in PHOEBE-scripter and similar to that outlined in the description of the JKTEBOP code (Southworth et al. 2004, and and references therein). A total of 15,000 simulations were performed for each binary. Since the iterated temperature of the secondary was equal to that resulting from the CK calibration to within 1σ, we did not attempt at any refinement of the solution. In the following, the temperatures derived from CK calibration for for both components of V54 were used for consistency. The uncertainties given in Table 6 arise from the uncertainties in $(B-V)$ listed in Table 4.

As expected from the orbital periods and the shapes of the light curves, both systems are well detached. The largest oblateness, amounting to 0.3%, is observed for the primary of V44 while for the secondary of V44 it is 0.1%. In the case of V54 the oblateness amounts to 0.01% and 0.003% for the primary and secondary, respectively. The residuals of the fits are shown in Fig. 2, and the final values of the iterated parameters are given in Table 4. The derived relative elements are unambiguous and well defined due to the totality of secondary eclipses. According to the obtained solution, totality lasts for 0.0049 P (i.e. 1.09 h) and 0.0227 P (i.e. 1.18 h) for V44 and V54, respectively. The location of both binaries and their components on the cluster CMD is shown in Fig. 3. The primary of V44 is located right at the turnoff, while the primary of V54 lies 0.4-0.5 mag below the turnoff. In both systems the secondary components are only slightly evolved stars, located about 4 mag below the turnoff.

A nonlinear least-squares fit to the observed velocity curves of V54 was obtained with the help of a code kindly made available by Guillermo Torres. While fitting, the orbital eccentricity and periastron angle were fixed based on the photometric solution. The observations and the orbital solutions are shown in Fig. 4, and the derived orbital parameters are listed in Table 5 together

with formal errors returned by the fitting routine. Table 5 also lists the standard deviations from the orbital solution σ_p and σ_s which are a measure of the precision of a single velocity measurement. An orbital solution with eccentricity and periastron angle included among the fitted parameters produced e=0.1411±0.0029 and ω=236.8±1.0. Both of these values are incompatible with the light curves, but the corresponding $M\sin^3 i$ values ($M_p \sin^3 i$=0.726±0.014$M_\odot$ and $M_s \sin^3 i = 0.555 \pm 0.007) M_\odot$) are identical to those obtained for fixed e and ω (the only difference is a slight reduction of the errors). Thus, the derived masses can be regarded as entirely reliable.

Upon combining data from Tables 4 and 5 we obtained the absolute parameters of the components of V54 listed in Table 6.

We note that the derived systemic velocity of V54 agrees well with the radial velocity of M55, which according to Harris (1996) is equal to 174.7 ± 0.3 km/s. Lane at el. (2010) list a slightly larger value ($V_{rad} = 177.37 \pm 0.13$ km/s), but their data also show that at a projected distance of 3-5 arcmin from the core the velocity dispersion amounts to about 2.5 km/s.

As V44 is a single-line binary, we could determine its mass function only. Using data from Table 3 we obtained $f(m)$=0.0891±0.0070$M_\odot$ and $m_s sin(i) = 0.447(m_s + m_p)^{2/3} \pm 0.017 M_\odot$ with the rms of residuls from the fit amounting to 1.9 km/s. The derived systemic velocity, $V\gamma = 179.05 \pm 0.46$ km/s, confirms the radial-velocity membership of V44 in M55 (Lane at el. 2010).

In the V band the primary of V44 is by 0.5 mag brighter the primary of V54. Based on Dartmouth isochrones (Dotter et al. 2008), this implies a difference in masses of about 0.02 $M_\odot$ at the turnoff of M55. Hence, the mass of the primary of V44 can be estimated at $m_p^{V44} \approx 0.74 M_\odot$. From the mass function one gets $m_s^{V44} \approx 0.53 M_\odot$ - a value consistent with m_s^{V54} and the location of the secondaries of V44 and V54 on the CMD of the cluster (Fig. 3).

4 Age and distance of V54

The fundamental parameters listed in Table 6 allow for a determination of the age of M55 via comparison with stellar isochrones. The following analysis has been carried out using isochrones from Dartmouth (Dotter et al. 2008) and Victoria-Regina (VandenBerg et al. 2012). These isochrones share similar physical assumptions, including nuclear reaction rates and opacities. The most significant difference is that the Dartmouth models include the effects of the diffusion of He and metals whereas the Victoria-Regina models include the diffusion of He but not metals. In both cases, the full effect of diffusion is mitigated near the surface (see the respective papers for further details). The Dartmouth isochrones adopt a constant α-enhancement factor (in this case [α/Fe]=+0.4 is assumed) whereas the Victoria-Regina models are based on an observationally-motivated, element-specific α-enhancement, amounting to [α/Fe] $\simeq +0.33$.

As the results obtained from the two sets of models turned out to be consistent with each other at 1σ-level, in the following we only report those based on Dartmouth isochrones. Fig. 5 shows a side-by-side comparison of the mass-radius plane containing V54 and the CMD from a region surrounding V54, to which we fitted isochrones using the reddening value $E(B-V) = 0.115$ from Section 3. Qualitatively, the $M-R$ diagram indicates an age of 14-15 Gyr for the primary and a younger age for the secondary. The CMD comparison favors an age of 13-14 Gyr - in agreement with the mass-radius relation of the secondary. We note that the age derived from the mass-radius relation is free from

uncertainties in distance and extinction that plague ages derived via isochrone fitting to the CMD.

A quantitative age analysis was performed for the components V54 following the technique described by Kaluzny et al. (2013) to study three binary systems in M4. Briefly, the method densely samples the $(M-R)$ or $(M-L)$ plane in both dimensions for each component separately, and finds the age of an isochrone that matches the properties of the sampled point. Thus generated age ensembles may be visualized in the form of histograms, as in Kaluzny et al. (2013), or mass-age diagrams (Fig. 6). The latter show ellipses composed of points which on $(M-R)$ or $(M-L)$ plane are 1σ-distant from the points specified by the solutions given in Table 6, where $\sigma^2 = \mathrm{err}(M/M_\odot)^2 + \mathrm{err}(R/R_\odot)^2$ for the $(M-R)$ plane and likewise for the $(M-L)$ plane; $\mathrm{err}(M/M_\odot)$, $\mathrm{err}(R/R_\odot)$ and $\mathrm{err}(L/L_\odot)$ being the standard errors of M, R and L from Table 6.

The ellipses for the primary in Fig. 6 are much smaller than those for the secondary, setting tighter limits for the age of V54. This is to be expected, as the primary sits just below the main sequence turnoff and evolves relatively quickly, while the secondary is located well down the 'unevolved' main sequence (Fig. 3), where the structure of the star changes very slowly with time. Each of the four ellipses in Fig. 6 defines a range of ages achieved by stars whose parameters differ from those listed in Table 6 by at most one standard error. Thus, a fair estimate of the age of V45 is the common part of the four ranges. The limits 13.3 – 14.7 Gyr derived in this way are compatible with the age of 13.5±1.0 Gyr obtained by Dotter et al. (2010) by isochrone fitting to HST data.

For stellar parameters from Table 6, the CK calibration gives bolometric corrections in V of 0.126 ± 0.005 mag for the primary and 0.230 ± 0.020 mag for the secondary. Using $M_\odot^{bol} = 4.755$[§] , we get absolute $V-$luminosities $M_{Vp} = 4.53 \pm 0.05$ mag and $M_{Vs} = 6.93 \pm 0.08$ mag, corresponding to apparent distance moduli $\mu_p = 13.87 \pm 0.05$ mag and $\mu_s = 14.00 \pm 0.08$ mag. The mean modulus of 13.94±0.05 mag agrees reasonably well with 14.03 mag obtained from CMD fitting and with 13.88 mag found by Dotter et al. (2010). Assuming $A_V = 3.1 \times E(B-V)$, the dereddened modulus is 13.58 mag.

The combination of CMD and mass-radius relation provide some leverage on the He content of M55. An initial He mass fraction of Y$\sim$0.25 has been assumed in the preceding analysis. However, there is at least one claim of a higher initial He mass fraction, Y=0.274 ± 0.016, based on star counts and the R-parameter (Vargas Alvarez & Sandquist 2007). In order to test this claim, the analysis carried out above was redone using Dartmouth isochrones with Y=0.27. Ages derived for Y=0.27 from the mass-radius relation yield a 1.8 Gyr reduction in the age of the primary. This is entirely consistent with composition-sensitivity tests performed by Kaluzny et al. (2013; their Section 6 and Table 14) and we refer the reader to that paper for further discussion of changes in chemical composition to the ages determined via mass-radius analysis. The position of isochrones through the turnoff and subgiant branch in the CMD are insensitive to modest changes in the initial He content at fixed age and metallicity (see, e.g., Figure 1 of Dotter, Kaluzny, & Thompson 2009). Hence the CMD of M55 will still favor an age of $\sim$14 Gyr with Y=0.27. The consistency found between mass-radius, mass-luminosity, and CMD fitting described in this section argues in favor of an initial Y$\sim$0.25 for M55.

[§] Mamajek's Star Notes, https://sites.google.com/site/mamajeksstarnotes/basic-astronomical-data-for-the-sun

5 Summary

We have analysed photometric and spectroscopic observations of the eclipsing binaries V44 and V54 in M55. V54 is an SB2 system, and we obtained absolute parameters of the components of this system, leading to an estimate of age and distance modulus of the cluster. The resulting age of 13.3 – 14.7 Gyr derived from $M-R$ and $M-L$ diagrams is compatible with the age 13 – 14 Gyr obtained from CMD fitting with Dartmouth or Victoria-Regina isochrones. Apparent distance moduli derived with the same two methods and the same two sets of isochrones are also compatible within the errors.

The best chance to tighten the age limits is offered by the mass-radius relation, which is independent of uncertainties in distance and extinction that plague ages obtained via isochrone fitting to the CMD. Since at the location of the primary on the $M-R$ plane the isochrones are almost perpendicular to the mass axis (that's why the corresponding ellipses in Fig. 6 are very narrow), the age uncertainty arises mainly from the error in the mass of the primary. The only way to reduce it is by taking additional spectra of V54. Thompson et al. (2010) estimate that doubling of the present set of velocity measurements would improve the mass estimates by 33 per cent.

The uncertainty of the location of V54 components on the $M-L$ plane is mainly due to the relatively poor accuracy of their luminosities which were found using absolute radii from Table 6 and effective temperatures estimated from $(B-V)-T_{eff}$ calibration of Castelli and Kurucz (2004). Unfortunately, the existing empirical calibrations are poorly defined for low mass stars with $[\mathrm{Fe/H}]<-1.5$ (Casagrande et al. 2010; Gonzalez-Hernandez & Bonifacio 2009). A significant improvement is expected when results from the GAIA astrometric mission will become publicly available. Also our determination of the distance to M55 depends heavily on the adopted teperature scale. A better accuracy could be achieved based on the surface brighness in V, which is known to tightly correlate with the $V-K$ color (Di Benedetto 2005). Given that V54 is located in the outer uncrowded part of the cluster, accurate near-IR photometry of these systems with large telescopes is entirely feasible.

Independent and potentially more accurate estimates of age and distance of M55 may follow from the analysis of the V44 system, whose primary is more evolved than the primary of V54 (see Fig. 3). While the secondary of V44 is too faint to measure its velocity in the visible domain, it seems to contribute enough light for successful measurements in the near IR. Accurate parameters of both systems could yield not only tight age limits, but also impose useful constraints on the primordial He content of the cluster.

The age we derived for M55 is by ~ 2 Gyr older than the ages we obtained from the analysis of eclipsing binaries in 47 Tuc (Thompson et al. 2010) and M4 (Kaluzny et al. 2013). This can be compared with recent result of Hansen et al. (2013) who, based on cooling sequences of white dwarfs, found that NGC 6397 ([Fe/H]=-2) is about 2 Gyr older than 47 Tuc. Hansen et al. stress the benefits of deriving ages from WDs, which are largely insensitive to metallicity, but are still subject to uncertainties in distance and reddening. In our case, sensitivity to metallicity is present but the uncertainties in distance and reddening are not. Since M55 and NGC 6397 have very similar metallicities, it is significant that these two more-or-less independent methods arrive at a similar age difference between metal-poor and metal-rich globular clusters.

Acknowledgements. JK, MR and WP were partly supported by the

grant DEC-2012/05/B/ST9/03931 from the Polish National Science Center. We thank Dr. Joao Alves for sending us the information about reddening in the M55 region. This series of papers is dedicated to the memory of Bohdan Paczyński.

REFERENCES

Alvarez, C. A. V., and Sandquist, E. L. 2007, *Astron. J.*, **134**, 825.
Alves, J., Lombardi, M., and Lada, J. C 2014, *arXiv:1401.2857v1*, , to be published in Astron. Astrophys..
Bernstein, R., Shectman, S. A., Gunnels, S. M., Mochnacki, S., and Athey, A. E. 2003, *Instrument Design and Performance for Optical/Infrared Ground-based Telescopes, eds. Masanori Iye and Alan F. M. Moorwood. Proceedings of the SPIE*, **4841**, 1694.
Carretta, E., Bragaglia, A., Gratton, R., and Lucatello, S. 2009, *Astron. Astrophys.*, **505**, 139.
Carretta, E., Bragaglia, A., Gratton, R., Lucatello, S., Bellazzini, M., and D'Orazi, V. 2010, *Astrophys. J. Letters*, **712**, 21.
Casagrande, L., Ramírez, I., Meléndez, J., Bessell, M., and Asplund, M. 2010, *Astron. Astrophys.*, **512**, 54.
Castelli, F., Kurucz, R. L. 2004, arXiv:astro-ph/0405087.
Claret, A. 2000, *Astron. Astrophys.*, **363**, 1081.
Coelho, P., Barbuy, B., Meléndez, J., Schiavon, R. P. and Castilho, B. V. 2005, *Astron. Astrophys.*, **443**, 735.
Di Benedetto, G.P. 2005, *MNRAS*, **357**, 174.
Dotter, A., Chaboyer, B., Jevremović, D. et al. 2008, *Astrophys. J. Suppl. Ser.*, **178**, 89.
Dotter, A., Kaluzny, J. and Thompson, I. B. 2009, *The Ages of Stars, Proceedings of the 258th Symposium of the IAU, Eds. E. Mamajek, D. Soderblom, and R. Wyse*, , 171.
Dotter, A., Sarajedini, A., Anderson, J., Aparicio, A., Bedin, L. R. et al. 2010, *Astron. J.*, **708**, 698.
González-Hernández, J. I. and Bonifacio, P. 2009, *Astron. Astrophys.*, **497**, 497.
Hansen, B. M. S., et al. 2013, *Nature*, **500**, 51.
Harris, W. E. 1996, *Astron. J.*, **112**, 1487 (2010 online edition).
Kaluzny, J., Thompson, I. B., Krzeminski, W. and Pych, W. 1999, *Astron. Astrophys.*, **350**, 469.
Kaluzny, J., Thompson, I. B., Krzeminski, W., et al. 2005, *Stellar Astrophysics with the Worlds Largest Telescopes, ed. AIP Conf. Proc.*, **752**, 70.
Kaluzny, J., Thompson, I. B., Krzeminski, W. and Zloczewski, K. 2010, *Acta Astron.*, **60**, 245.
Kaluzny, J., Thompson, I. B., Rozyczka, M. et al. 2013, *Astron. J.*, **145**, 43.
Kelson, D. D. 2003, *P.A.S.P.*, **1125**, 688.
Lafler, J. and Kinman, T. D. 1965, *Astrophys. J. Suppl. Ser.*, **11**, 216.
Lane, R. R., Kiss, L. L.; Lewis, G. F. et al. 2010, *MNRAS*, **401**, 2521.
Prša, A., and Zwitter, T. 2005, *ApJ*, **628**, 426.
Richter, P., Hilker, M. and Richtler, T. 1999, *Astron. Astrophys.*, **350**, 476.
Schechter, P. L., Mateo, M. and Saha, A. 1993, *P.A.S.P.*, **105**, 1342.
Schlafly, E. F., Finkbeiner, D. P.; Schlegel, D. J.; Jurić, M. Ivezić, Željko; et al. 2010, *Astrophys. J.*, **725**, 1175.
Schlegel D. J., Finkbeiner D. P. and Davis M. 1998, *Astrophys. J.*, **500**, 525.
Southworth, J., Maxted, P. F. L. and Smalley, B. 2004, *MNRAS*, **349**, 547.
Thompson, I. B., Kaluzny, J., Rucinski, S. M., et al. 2010, *Astron. J.*, **139**, 329.
VandenBerg, D. A., Bergbusch, P. A., Dotter, A., Ferguson, J. W., Michaud, G., Richer, J., and Proffitt, C. R. 2012, *Astrophys. J.*, **755**, 15.
Wilson, R. E. 1979, *Astrophys. J.*, **234**, 1054.
Wilson, R. E., and Devinney, E. J. 1971, *Astrophys. J.*, **166**, 605.
Zloczewski, K., Kaluzny, J., Rozyczka, M. et al. 2012, *Acta Astron.*, **62**, 357.
Zucker, S., and Mazeh, T. 1994, *Astron. J.*, **420**, 806.

Table 1: Times of minima for V44 and V54.

Star	E	Tmin [d] HJD-2450000	σ [d]	O-C [d]
V44	-687	588.73725	0.00137	-0.00036
V44	-674	616.89698	0.00130	-0.00051
V44	0	2076.86429	0.00173	-0.00189
V44	319	2767.85376	0.00140	0.00142
V44	366	2869.66077	0.00101	0.00212
V44	836	3887.74008	0.00070	-0.00006
V44	849	3915.89977	0.00039	-0.00016
V44	871	3963.55348	0.00390	0.00080
V44	872	3965.72231	0.00138	-0.00191
V44	1023	4292.80459	0.00066	0.00016
V44	1179	4630.71970	0.00037	0.00002
V54	0	663.67449	0.00213	0.00215
V54	238	2869.73600	0.00173	-0.00078
V54	428	4630.87478	0.00062	-0.00035
V54	428	4630.87550	0.00112	-0.00107
V54	465	4973.83301	0.00048	0.00011
V54	465	4973.83449	0.00104	-0.00137
V54	506	5353.86830	0.00052	0.00012
V54	506	5353.86750	0.00069	0.00092

Table 2: Radial velocity observations of V54

HJD -2450000	v_p [km/s]	v_s [km/s]	Phase	$(O-C)_p$ [km/s]	$(O-C)_s$ [km/s]
2871.6532	125.36	237.37	0.207	-0.86	-0.53
2872.6607	126.90	238.86	0.316	-0.74	2.82
2922.5065	219.00	118.64	0.693	-0.26	2.37
2923.4957	210.74	127.98	0.800	-0.51	1.24
2944.5042	154.07	202.33	0.066	-0.58	1.59
2946.4997	121.87	244.55	0.282	-1.90	3.44
3178.7800	132.97	226.52	0.341	0.18	-2.79
3180.7962	205.80	135.77	0.559	0.86	0.78
3182.8380	213.75	121.85	0.779	-0.07	-1.53
3206.6655	134.53	224.35	0.350	-0.35	-2.23
3210.6248	212.69	126.03	0.777	-1.38	2.97
3280.4991	127.70	236.88	0.315	0.13	0.74
3281.5346	161.52	189.97	0.427	0.76	-2.77
3282.5326	198.61	144.62	0.535	-0.10	1.49
3581.7421	209.19	134.09	0.815	-0.01	4.67
3582.7236	189.51	156.47	0.921	-0.17	1.53
3584.6869	139.41	222.42	0.132	0.26	1.42
3585.6744	124.05	245.53	0.239	0.54	4.09
3632.5485	124.88	241.14	0.296	-0.10	1.61
3635.5729	215.62	122.48	0.622	-0.19	1.69
3875.8479	203.24	138.00	0.544	1.91	-1.71
3877.8737	215.39	120.77	0.763	-0.12	-0.40
3891.8346	124.06	243.21	0.269	0.89	1.33
3937.6913	125.74	242.07	0.216	0.52	2.86
4648.7677	186.33	162.43	0.930	-1.18	4.66
4656.8090	211.28	127.79	0.798	-0.23	1.39
5389.7060	199.92	143.79	0.866	-0.70	3.15

Table 3: Radial velocity observations of V44

HJD -2450000	v_p [km/s]	HJD -2450000	v_p [km/s]
2838.6719	253.40	3892.8097	118.47
2839.6845	112.64	3937.7585	138.68
3179.9013	105.55	3937.8037	130.17
3180.8638	241.95	4258.8596	113.87
3280.5677	251.39	4314.7773	123.18
3281.6041	113.14	4333.5189	249.88
3282.5920	231.30	4655.7762	204.85
3580.7507	106.60	4656.7739	168.57
3877.8054	141.95	5038.7444	123.71
3891.7597	237.46		

Table 4: Photometric parameters of 54 and V44[a]

Parameter	V54	V44
i(deg)	89.050(27)	86.86(11)
r_p	0.04992(32)	0.15835(54)
r_s	0.02617(23)	0.06807(45)
e	0.133(5)	0[b]
ω (deg)	237.1(2)	0[b]
T_p (K)	6246[b]	6602[b]
T_s (K)[c]	4959(16)	4807(28)
$(L_p/L_s)_V$	10.80(23)	0.2326(54)
$(L_p/L_s)_B$	14.93(39)	0.
$\sigma_{rms}(V)$ (mmag)	83	75
$\sigma_{rms}(B)$ (mmag)	101	75
V_p (mag)[d]	18.399(7)	17.928(7)
V_s (mag)[d]	20.983(22)	21.391(27)
B_p (mag)[d]	18.933(6)	18.417(5)
B_s (mag)[d]	21.869(26)	22.370(34)
$(B-V)_{0p}$(mag)[e]	0.419(14)	0.374(18)
$(B-V)_{0s}$(mag)[e]	0.771(32)	0.864(45)

[a]Numbers in parentheses are the errors of the last significant digits.
[b]Assumed in fit.
[c]Result of PHOEBE iterations.
[d]The internal error from the photometric solution and profile photometry is given.
[e]The error includes the internal error from the photometric solution and profile photometry as well as errors of zero point of photometry and interstellar extinction.

Table 5: Orbital parameters of V54[a]

Parameter	Value
γ (km s^{-1})	174.62(15)
K_p (km s^{-1})	48.13(19)
K_s (km s^{-1})	62.92(60)
e	0.133[b]
ω (deg)	237.1[b]
σ_p (km s^{-1})	0.79
σ_s (km s^{-1})	2.50
Derived quantities:	
$A\sin i$ ($R_\odot$)	20.16(12)
$M_p \sin^3 i$ ($M_\odot$)	0.7259(154)
$M_s \sin^3 i$ ($M_\odot$)	0.5552(75)

[a]Numbers in parentheses are the errors of the last significant digits
[b]Assumed in fit

Table 6: Absolute parameters of V54

Parameter	Value
M_p ($M_\odot$)	0.726(15)
M_s ($M_\odot$)	0.555(8)
R_p ($R_\odot$)	1.006(9)
R_s ($R_\odot$)	0.528(5)
T_p (K)[a]	6246(71)
T_s (K)[a]	5020(95)
L_p^{bol} ($L_\odot$)	1.381(67)
L_s^{bol} ($L_\odot$)	0.159(12)

[a] Derived from the calibration of Castelli & Kurucz (2004). The errors reflect the uncertainties in $(B-V)$ from Table 4.

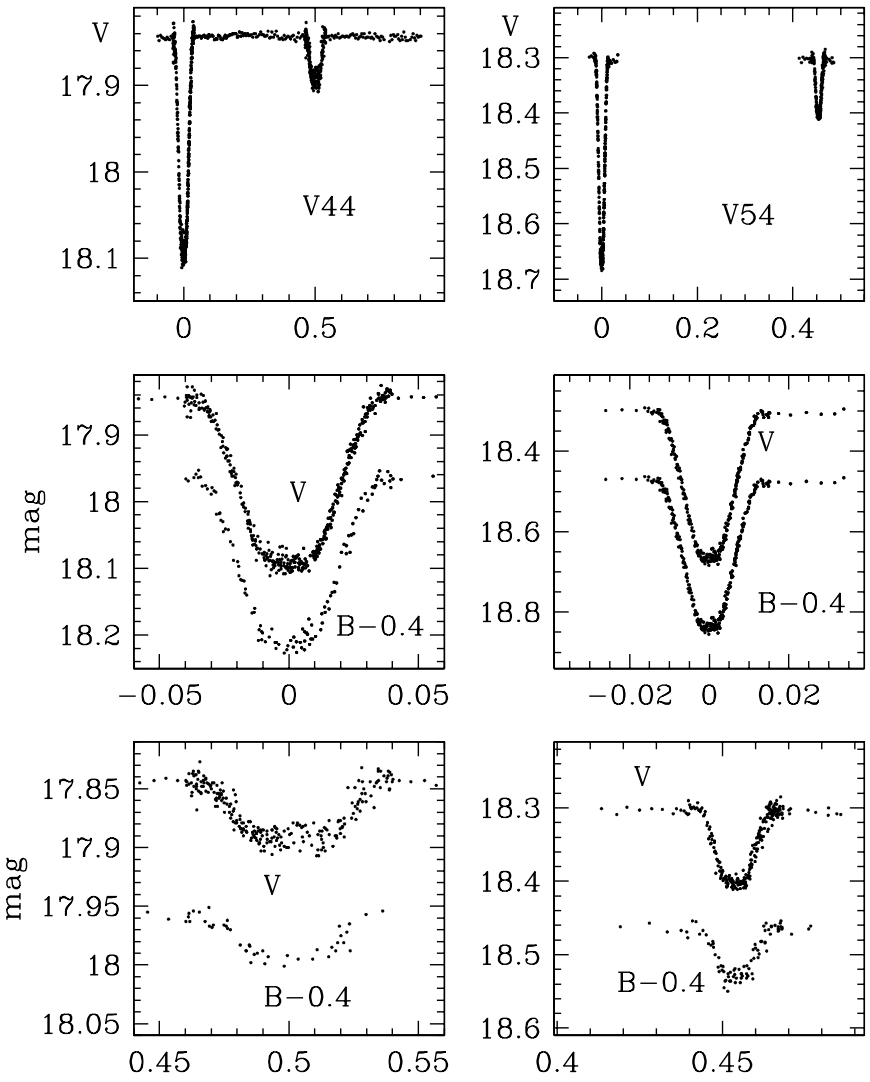

Figure 1: Light curves of V44 (left column) and V54 (right column) obtained with the du Pont telescope and the TEK5 CCD camera. The B-curves are shifted upwards by 0.4 mag.

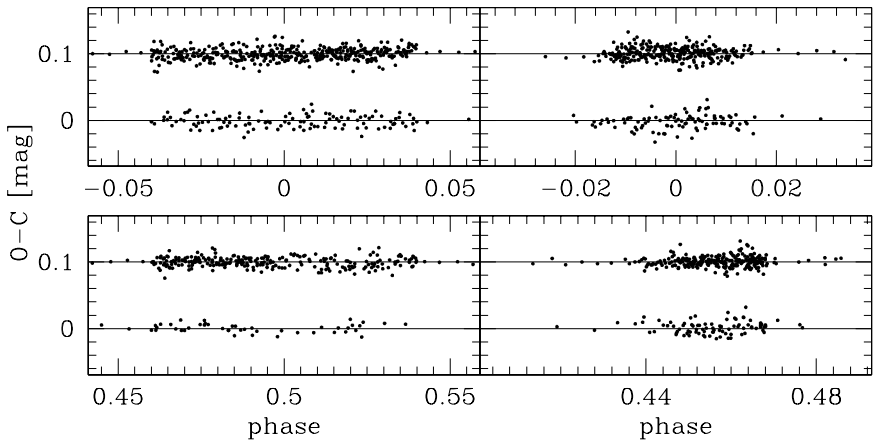

Figure 2: Residuals to the fits adopted for the analysis. Left panels: V44. Right panels: V54. In each panel, the lower sequence represents the B-residuals, and the upper one the V-residuals offset by 0.1 mag for clarity.

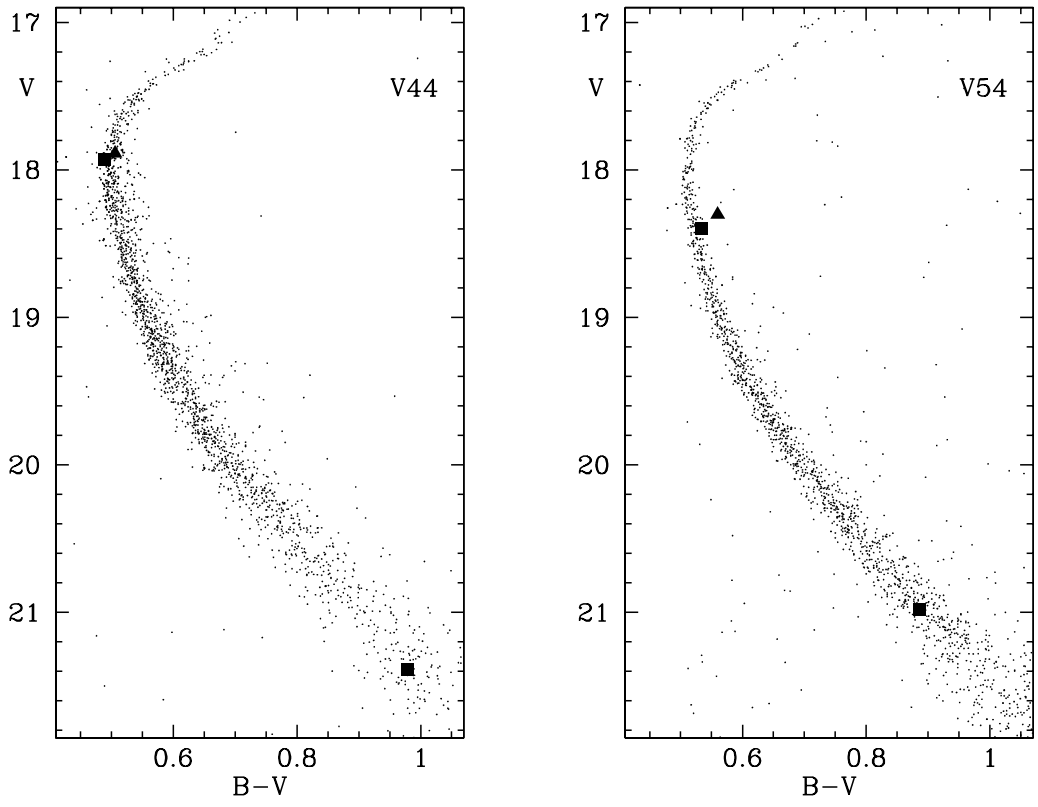

Figure 3: Color-magnitude diagrams of M55 with marked positions of V44 and V54 systems (triangles) and their components (squares). Stars in each panel are taken from the surroundings of the corresponding system.

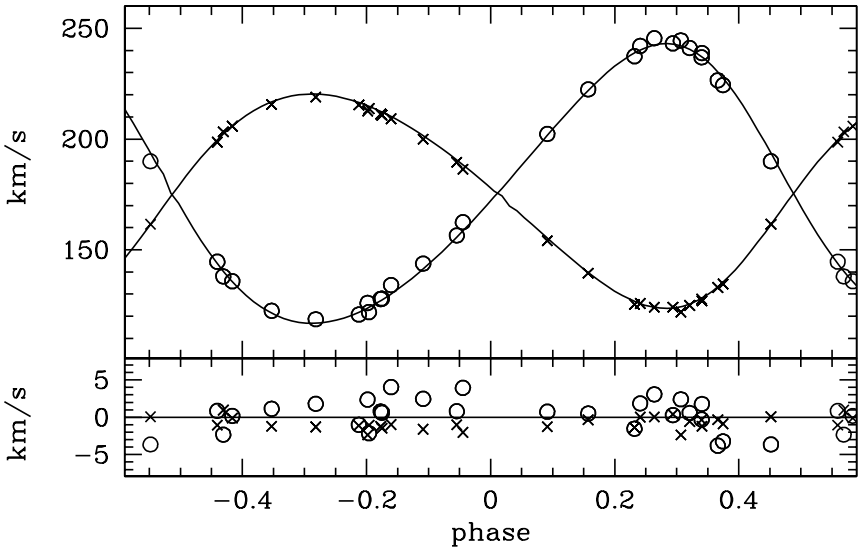

Figure 4: Velocity curve of V54 adopted for the analysis. Crosses and open circles denote, respectively, primary and secondary velocities (upper panel) and residuals to the fit (lower panel).

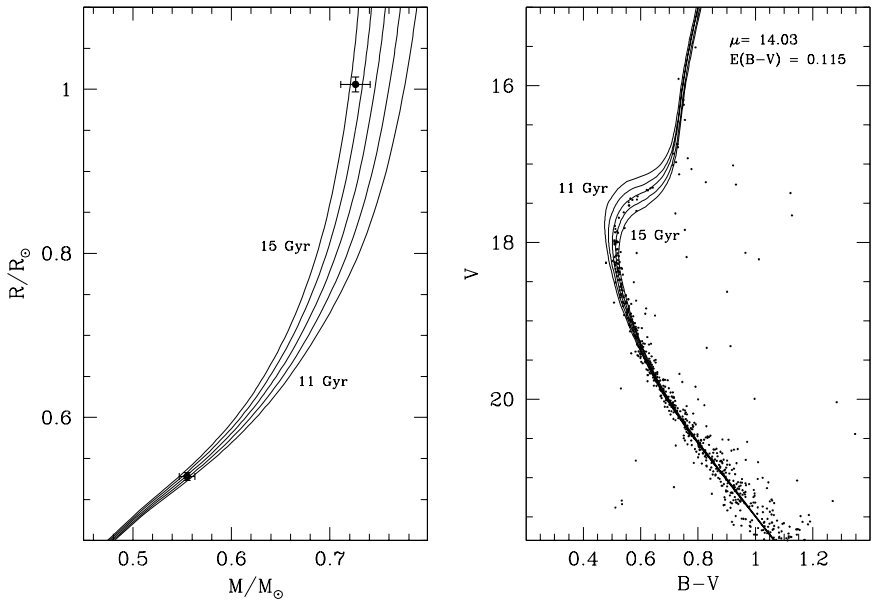

Figure 5: Left: Dartmouth isochrones (lines) at [Fe/H]=−2.0, [α/Fe]=+0.4 compared to the components of V54 (points with 1σ errors) in the mass-radius diagram. Right: The same isochrones transformed to the observational plane compared to the CMD from a region of M55 containing V54. The apparent distance modulus resulting from the fit is equal to 14.03 mag for $E(B-V)$=0.115 mag. To better visualize the isochrones, the stars shown are from a smaller area surrounding of V54 than the region used for the right panel of Fig. 3.

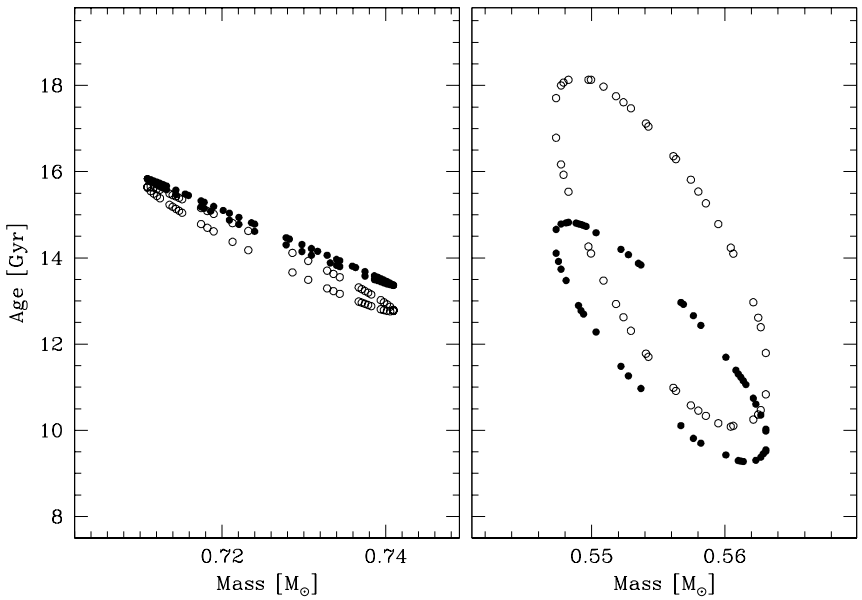

Figure 6: Mass-age diagrams for the primary (left) and the secondary (right) component of V54 based on Dartmouth isochrones. Results from the analysis of $(M-R)$ and $(M-L)$ planes are shown with dots and open circles, respectively (see Section 4 for a detailed explanation).